Energy 93 (2015) 683–696

Contents lists available at ScienceDirect

Energy

journal homepage: www.elsevier.com/locate/energy

Wave energy resource assessment in Uruguay

Rodrigo Alonso*, Sebastián Solari, Luis Teixeira

Instituto de Mecánica de los Fluidos e Ingeniería Ambiental, Facultad de Ingeniería, Universidad de la República, Uruguay

ARTICLE INFO

Article history:
Received 22 April 2015
Received in revised form
13 August 2015
Accepted 31 August 2015
Available online xxx

Keywords:
Renewable energy
Wave energy
Wave hindcast
Climate variability
Extreme events
Wave modeling

ABSTRACT

Marine energy sources are an untapped resource able to make a significant contribution to renewable and clean energy generation. In Uruguay, investment in renewable energy has experienced strong growth in recent years. Because the country is located in a microtidal zone, wave energy is the most promising marine energy resource. An assessment of its potential was conducted from a 31-year wave hindcast performed with the Wavewatch III® third-generation wave model forced by CFSR (Climate Forecast System Reanalysis) winds. The model was calibrated and validated with altimeter data and in situ measurements. The spatial distribution of the resource and its variability at different timescales were analyzed, as well as the correlation between the variability of the directional wave spectrum and several climate indexes. The extreme conditions that a wave energy converter should withstand were analyzed, and a new figure was defined to quantify the impact of extreme conditions on WEC (Wave energy converter) design and optimization. The obtained results show that although wave energy potential is moderate, it is fairly steady throughout the year, and the extreme waves are relatively benign. Therefore, wave energy is an attractive resource for integration into the country energy mix, contributing to its diversification and sustainability.

1. Introduction

The needs to meet the growing global energy demand and to address the concerns regarding energy security and the environmental consequences of global warming attributable to the use of fossil fuels has led to the development of many renewable energy projects worldwide [53]. In this context, marine energy sources are an untapped resource able to make a significant contribution to the development of a sustainable energy mix [52]. Among the five marine energy sources, namely, waves, currents, tides, thermal gradient and saline gradient, waves have the greatest potential [49]. Gunn and Stock-Williams [17] estimated that at 30 nautical miles offshore, the global ocean wave theoretical potential is 2.11 TW. The theoretical potential, which refers to the annual average of physical power that is hypothetically available, must be distinguished from the technical resource potential, which refers to the portion of a theoretical resource that can be captured using a specific technology.

WEC (Wave energy converter) technology has experienced accelerated development in recent years and is recognized as an industry in its own right. Currently, the most advanced projects are in the commercial demonstration stage [59], whereas several other projects are in the preliminary stages of development. A special feature of the present status of WEC technology is the coexistence of different systems [13], which differ in the principle used for harvesting energy, their location (off-shore, intermediate waters or near-shore) and their orientation relative to incident waves. Esteban & Leary [12] compared the developments in the field of wave energy with the recent development of the wind off-shore energy field. They estimated that WEC technology will be competitive after 2020 and that by 2050, 7% of global energy will be generated in the sea, mainly from waves, currents and offshore winds, employing approximately 1 million people.

Theoretical potential resource assessment is the mandatory first step to begin wave energy research. Global assessments (e.g. [17,39], provide a first idea of the theoretical potential at any point. However, to obtain accurate and detailed results that can be used as inputs of feasibility studies of wave farms, high resolution assessments using local information are required. Many studies have been conducted in different locations in recent years (e.g., [1–6,11,14]; [15,16] [26][28,30,33–35,37,38,40–47,56–58]; [61,62,63]. Except for a few works based exclusively on buoy data

* Corresponding author.
E-mail addresses: ralonso@fing.edu.uy (R. Alonso), ssolari@fing.edu.uy (S. Solari), luistei@fing.edu.uy (L. Teixeira).

http://dx.doi.org/10.1016/j.energy.2015.08.114
0360-5442/

(e.g. [30], high-resolution studies are based in wave hindcast databases because the in situ and altimetry measurements are generally not sufficient to sustain a comprehensive resource assessment that typically covers a large area (territorial sea of a country) and a long period of time (more than 10 years).

High-resolution studies are not only aimed at the analysis of the mean annual availability of the resource but also the analysis of its variability, typically by characterizing its annual cycle. Although the interannual variability is relevant when in the characterization of an energy source, most studies do not perform the analysis [40]. Moreover, most of the studies that do analyze interannual variability limit themselves to the analysis of the variability of the total energy (generally using the coefficient of variation or an equivalent approach; e.g. [3,14,33,35,41,46], or of the omnidirectional spectrum (e.g. [40,56], overlooking the variability of the directional spectrum, which is an important factor when choosing and optimizing a WEC for a particular place [30]. Few studies have linked the interannual variability of the wave energy resource with global climate indexes (e.g., [35,40,41]).

Another aspect that has not been systematically studied, even though it has shown to be an important factor for feasibility studies [23], is the characterization of the extreme conditions that a WEC would have to withstand in a given place. Except for [56] who conducted a complete extreme value analysis, and [19] who analyzed the 100-year return conditions, recent studies have analyzed only particular extreme storms (e.g. [15], or the maximum value registered during the hindcast period (e.g. [9], uses the maximum value of the 10 years series for their global analysis).

Uruguay has no exploitation of fossil fuels. To reduce the dependence of its prices and availability, the country is undergoing the process of diversification of the energy mix towards renewable and native sources. The government's short-term objective is to reach 50% of the primary energy mix obtained from these sources ([36]). In this way, wind energy [18], solar ([51]), biomass and micro-hydro developments are adding to the traditional and limited hydropower. In the long term, and taking account of the Uruguayan maritime domain, wave energy appears as an interesting alternative to continue increasing the weight of renewable and native sources in the national energy mix.

Global assessments shows that in deep waters, the theoretical wave energy potential of the Atlantic Ocean close to Uruguay is between 20 and 30 kW/m [17,39]. Although this value does not attract attention on a global map, which highlights the west coasts of the continents in mid and high latitudes (e.g., U.K., Chile and Australia), the zone is still catalogued as a good offshore location, according to Ref. [13].

In this paper, an analysis of the wave energy potential of the Uruguayan coasts is presented. To this end, a local high resolution wave hindcast was implemented and calibrated. Then, a detailed assessment of wave energy resources was performed, analyzing the spatial distribution and temporal variability at different time scales. Additionally, the issues previously raised were addressed, namely, the full directional spectrum was analyzed and its variability was correlated with several global climatic indexes, and a new index was defined to quantify the impact of extreme wave conditions on the design and optimization of a WEC for local applications.

The remainder of the paper is organized as follows. In Section 2, the study area is introduced (2.1), the wave model and its calibration are described (2.2 and 2.3), and the methodologies used to characterize wave energy resources are defined (2.4). In Section 3, calibration and validation results are shown (3.1), and the following issues are analyzed: wave climate and spatial distribution (3.2), temporal variability (3.3) and extreme conditions (3.4). Finally, the conclusions are summarized in Section 4.

2. Materials and methods

2.1. Study zone

The study zone includes the Río de la Plata and the Uruguayan waters in the Atlantic Ocean (Fig. 1). The Río de la Plata is a large estuary formed by the confluence of Paraná and Uruguay rivers. It is 290 km long and has a NW–SE orientation. In the outer zone, the estuary is wide (O(200 km)), and the depth varies between 10 and 20 m, whereas in the intermediate and inner zone, it is narrower (O(50 km)) and shallower (O(5 m)). The Uruguayan Atlantic Shelf is wide, with the coast oriented perpendicular to SE. Taking the 200 m iso-depth as a reference, the width of the continental shelf varies between 140 and 180 km. Between the coast and the 50 m iso-depth, the presence of shoals and pits form an irregular bathymetry.

2.2. Wave model

The hindcast was performed with a third-generation wave model forced with reanalysis winds. This class of models represents the time evolution of the wave spectrum, based on the propagation, generation, wave–wave interactions and dissipations off all spectral wave components individually. Third-generation models allow for the modeling of waves under more realistic and arbitrary conditions than the idealized cases assumed by parametric wave models. Furthermore, they improve on their predecessors (first- and second-generation wave models) because the spectrum is free to develop without any shape imposed a priori (see e.g., [24,29].

2.2.1. Description

The model used for wave hindcasting was the third-generation wave model WAVEWATCH III® version 3.14 [55],[1] which solves the random phase spectral action density balance equation for wavenumber-direction spectra,

$$\frac{\partial N}{\partial t} + \nabla_x \cdot (c_g + U)N + \nabla_s \cdot c_s N = \frac{S}{\sigma}, \tag{1}$$

where $N = F/\sigma$ is the wave action spectral density, F is the spectral energy density, σ is the relative frequency, ∇_x and ∇_s are the differential operators in space and the spectrum, respectively, c_g is the group velocity, U is the mean horizontal current velocity, c_s is a characteristic velocity in the spectral space and S is the sum of the wave energy source and sink terms, as detailed in Eq. (2),

$$S = S_{in} + S_{nl} + S_{ds} + S_{bot} + S_{db}, \tag{2}$$

where S_{in} is the energy supplied by the wind, S_{nl} is the energy transfer between spectral bins due to quadruplet non-linear interactions, S_{ds} is the energy dissipation in deep waters (white-capping), S_{bot} is the energy dissipations due to bottom friction and S_{db} is the dissipation due to bottom-induced breaking.

The selection of the parametrization used to represent $S_{in} + S_{ds}$ is described in Section 2.3. To calculate S_{nl}, Discrete Interaction Approximation (DIA [21], was used. To represent S_{db}, the parametrization of Ref. [60] was considered using the McCowan criteria to define the maximum non-breaking individual wave height, and JONSWAP parametrization [22] was used for S_{bot} (see Ref. [55] and references therein for details of the parametrizations).

[1] Source code available at http://polar.ncep.noaa.gov/waves/wavewatch/wavewatch.shtml (last visited on August 2nd 2015).

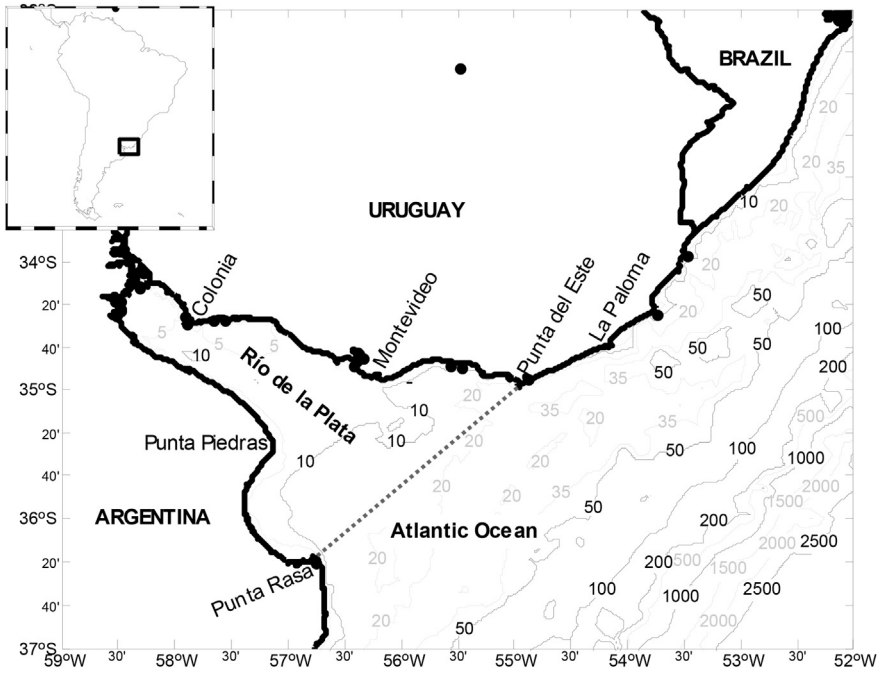

Fig. 1. Location of the study area and its bathymetry.

Table 1
Computational grids: covered domain, spatial resolution and time steps.

	Domain (SW corner-NE corner)	Δlon	Δlat	Δt_g(s)	$\Delta t_{p,r}$(s)	$\Delta t_{k-\theta}$(s)	Δt_s(s)
Global	(180 W,78 S)–(180 E, 78 N)	1.25°	1°	3600	1300	3600	300
Regional	(66 W,42 S)–(42 W, 22 S)	5′	5′	720	300	720	20
Local	(58.77 W,36.17 S)–(52.02 W, 32.52 S)	1′	1′	180	60	180	20

2.2.2. Computational grids

A multi-grid approach [55] with three grids (global, regional and local) was used. The area covered by each grid, the spatial resolution and the different time steps used are shown in Table 1. The different time steps are those used in the fractional step method [55], where Δt_g is the global time step, by which the entire solution is propagated in time and input winds are interpolated, $\Delta t_{p,r}$ and $\Delta t_{k-\theta}$ are the time steps for spatial and intra-spectral propagation, respectively, and Δt_s is the time step for the integration of the source terms.

The spectrum was discretized in 24 directions uniformly distributed and 25 frequencies distributed as a logarithmic grid covering the range of 0.0418 Hz–0.4114 Hz. The third-order ultimate quickest numerical scheme [10,31,32] was used to solve the spatial and intra-spectral propagations, and the averaging technique was used to alleviate the Garden Sprinkler Effect [54].

2.2.3. Input and calibration data

The wave data used in the calibration and validation of the model are in situ measurements obtained at two points and altimetry data from the L2P database of the Globwave project (see www.globwave.org). In situ measurements were obtained by means of a Datawell Waverider buoy located at coordinates 35°40′S, 55°50′W and an ADCP (Acoustic Doppler Current Profiler) located close to the Montevideo coast at coordinates 34°58′S, 56°10′W. Both in situ measurements are located inside the estuary; therefore, altimetry data were the only data available for calibration in the Atlantic region. The location of the buoy and the ADCP and satellite tracks in the study zone are shown in Fig. 2.

Wind data were obtained from the Climate Forecast System Reanalysis[2] [48], hereinafter CFSR, which is the latest atmospheric reanalysis of the NCEP (National Center for Environmental Predictions) and has higher spatial and temporal resolutions than previous reanalysis, providing a valuable resource to develop a long-term hindcast database for wind waves [7]. The spatial resolution of the wind fields is 0.5° × 0.5°, and the period covered is 1980–2010.

2.3. Calibration and validation

There are three packages available in WWIII v3.14 for the parametrization of the input and dissipation terms ($S_{in} + S_{ds}$): WAM-3, Tolman and Chalikov and WAM-4 and variants (see Ref. [55] for details). To select the package that gives the best results for this particular study, a period of six months was simulated using each of the packages. Then, the obtained results for the significant wave height (H_s) were compared with the altimetry data in the Atlantic region. This area was prioritized because the wave power there is more promising than in the estuary. In situ measurements taken in the estuary were then used only for verification purposes.

[2] Data was accessed through the CISL Research Data Archivehttp://dx.doi.org/10.5065/D6513W89 (last visited on August 2nd 2015).

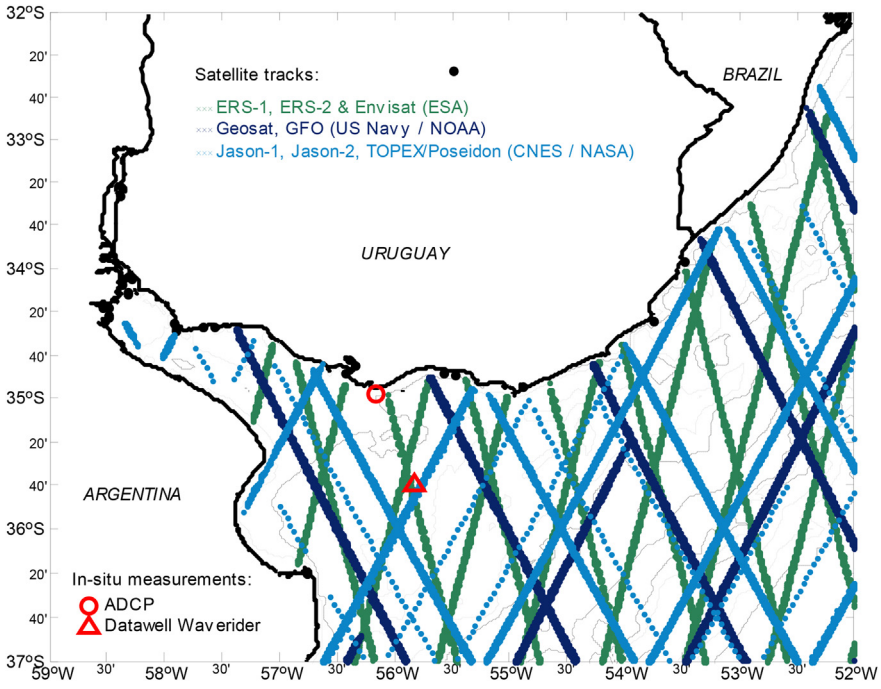

Fig. 2. Satellite tracks and locations of in situ measurements.

Bias, RMSE (Root Mean Square Error) and SI (Scatter Index) were the error metrics used to assess model performance,

$$Bias = \overline{y_m - y_o}, \tag{3}$$

$$RMSE = \sqrt{\overline{(y_m - y_o)^2}}, \tag{4}$$

$$SI = \frac{\sqrt{\left(\left(y_m - \overline{y_m}\right) - \left(y_o - \overline{y_o}\right)\right)^2}}{\overline{y_o}} \times 100, \tag{5}$$

where y is the analyzed magnitude (H_s in this case), and subindexes m and o refer to the model and observation, respectively. The period simulated was 1/1/2005–30/6/2005, and 2223 data points were obtained for comparison. According to the spatial and temporal resolution of the model (Table 1), the space and time distances between observed (satellite) and modeled data are less than 1 km and 30 min, respectively.

Once the parametrization of $S_{in} + S_{ds}$ giving the best results was selected, the calibration of the model was performed. The calibration included tuning the dimensionless coefficient (C_{ds}) involved in the parametrization of whitecapping (S_{ds}), that is, the process usually considered to be a tuning knob in this type of wave model [64]. Finally, the validation of the model was performed based on the simulation of a different period: 1/7/2005–31/12/2005. Table 2 includes the final configuration of the model.

2.4. Model outputs and analysis methodology

A total of 31 years (between 1980 and 2010) were simulated after the model was calibrated and validated. The model outputs are 3-hourly sea state parameters: significant wave height, mean and peak period, mean and peak directions and omnidirectional wave power calculated as,

$$P = \int_0^{\infty} \int_0^{2\pi} F(\sigma, \theta) \cdot C_g(\sigma) d\sigma d\theta, \tag{6}$$

where F is the spectral energy density, and C_g is the module of the group velocity. Additionally, 3-hourly full directional spectrums were obtained for the 22 virtual buoys shown in Fig. 3. Most of them (17 buoys) are distributed along the Atlantic coast in areas with depths approximately 20 m, whereas the remaining 5 buoys are dispersed inside the estuary, 2 of them corresponding to the location of the ADCP (PB in Fig. 3) and the Waverider Buoy (HV in Fig. 3).

2.4.1. Temporal variability

The variability of the wave energy resources at different timescales must be considered in any prospective energy extraction project. The variation coefficient (COV) obtained by dividing the standard deviation (σ) by the mean (μ) of a series is a simple indicator that can be applied at different timescales. The COV (coefficient of variability) is calculates as,

Table 2
Synthesis of the final configuration of the wave model.

Physical processes	Parametrization selected	Parameters
Wave growth and decay due to the action of winds ($\boldsymbol{S_{in}}$) in addition to dissipation ($\boldsymbol{S_{wc}}$)	WAM-4 and variants (ST3)	$C_{ds} = -1.5$ and the rest of the parameters by default
Non-linear resonant interactions ($\boldsymbol{S_{nl}}$)	DIA approximation	Default parameters values (see Ref. [55])
Dissipations due to bottom friction ($\boldsymbol{S_{bot}}$)	JONSWAP	Default parameters values (see Ref. [55])
Dissipations due to bottom-induced wave breaking ($\boldsymbol{S_{db}}$)	Batjjes-Jansenn	Default parameters values (see Ref. [55])

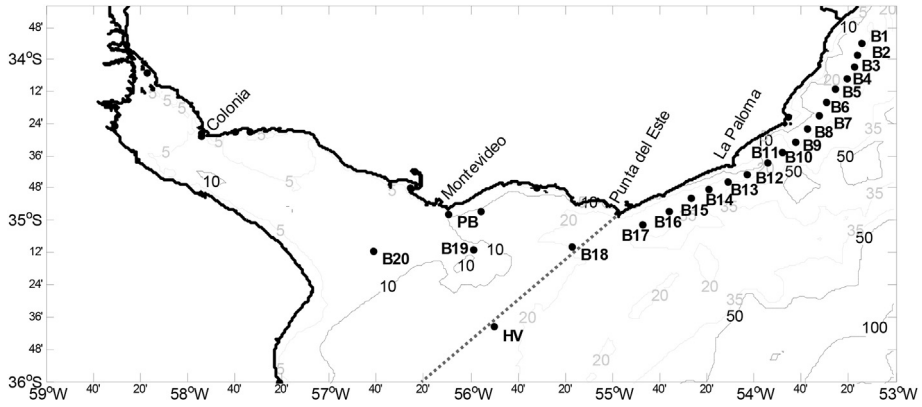

Fig. 3. Locations of the virtual buoys. HV (Hidrovía) corresponds to the location of the Waverider Buoy in the outer Rio de la Plata. PB (Punta Brava) corresponds to the location of the ADCP in front of Montevideo.

$$COV = \frac{\sigma}{\mu} = \frac{\overline{\left[(P-\overline{P})^2\right]}^{0.5}}{\overline{P}}, \tag{7}$$

where the over bar denotes the average, and P is the wave power estimated on a specific time scale. The variation coefficient is calculated at each grid point for the original 3-hourly series (COV 3h), for the monthly averages series (COV monthly) and the annual averages series (*COV annually*). Additionally, the SV (seasonal variability) index and MV (monthly variability) index proposed by Ref. [9] are calculated,

$$SV = \frac{P_{S1} - P_{S4}}{\overline{P}}, \tag{8}$$

$$MV = \frac{P_{M1} - P_{M12}}{\overline{P}}, \tag{9}$$

where P_{S1} and P_{S4} are the mean wave power of the most and least energetic season, respectively. In the same way, P_{M1} and P_{M12} are the mean wave power of the most and least energetic month, respectively.

To deepen the understanding of the causes of the wave energy variability, the correlation between wave energy variability and climatic indexes affecting the South Atlantic Ocean is analyzed. To this end, the linear correlation between the mean monthly energy anomaly and the indexes anomaly is calculated. However, atmosphere circulation variability may affect the total mean monthly wave energy and the period and the direction of the waves, affecting the efficiency of any given WEC. The linear correlation between the climatic indexes and monthly anomaly of the wave energy contained at every spectral bin (that is, at every period and direction bin of the directional wave spectrum) is also calculated. The following indexes are used for this analysis: El Niño 3.4 (NINO), SOI (Southern Oscillation Index), Antarctic Oscillation (AAO or SAM) and TSA (Tropical South Atlantic Index). Index anomalies are provided by the National Oceanic and Atmospheric Administration of the US (NOAA).[3]

2.4.2. Extreme wave climate

When designing a WEC, one has to take account of both operational (exploitation) and extreme conditions, i.e., the WEC device structure, its foundation and its mooring system must be designed to withstand the actions that may be produced by extreme events during their lifetime. Then, the ideal case is a situation where operational and extreme conditions are similar, so once the WEC is optimized for operational conditions, no significant investment is required to provide the WEC with additional resistance to withstand extreme events. This is rarely the case, and one requires some indication of how severe the extreme design conditions would be in comparison to the operational conditions. To assess this [19], is revisited, and a new index is proposed.

Hagerman [19] proposed the use of the FOM (Figure of Merit) for the evaluation of the wave energy potential in several US coastal areas. FOM was defined as the division of the mean annual wave energy flux in operational sea states ($\overline{EF}$) over the 100-year maximum wave height ($H_{max,100}$).

$$FOM = \frac{\overline{EF}}{H_{max,100}} \tag{10}$$

We define the exploitation to extreme ratio (ETER (Exploitation to extreme ratio); eq. (11)) by dividing the significant wave height representative of the sea conditions that provide more energy in a year (referred to as exploitation H_s or H_e) by the significant wave height representative of the most severe extreme events that the project should be able to withstand (referred to as design H_s or H_d). The smaller this ratio is, the higher the difference between the operational and extreme conditions used for the design of the WEC (i.e., ETER could be interpreted as the structural efficiency of the WEC structure, being equal to one when exploitation and extreme conditions are the same).

$$ETER = \frac{H_e}{H_d} \tag{11}$$

Here, the exploitation significant wave height (H_e) is defined as the significant wave height corresponding to the maximum of the annual wave energy distribution (see, e.g., Fig. 10), whereas H_d is defined as the significant wave height of the 112-year return period, corresponding to a 0.2 failure probability in a 25-year lifetime (in agreement with the return period used for the design of off-shore structures, see, e.g., [27]).

The ETER index was calculated for every point in the computational grid, allowing for comparison between different places inside the study area. To enable comparisons with previous studies of different areas, the 10-year return period, H_s (H_{10}), was calculated and mapped. In the calculation of H_d and H_{10}, the Probability Weighted Moments method was used to fit a GEV (Generalized Extreme Value distribution) to the annual maxima series [25]; see Appendix 1 for details).

[3] Data was accessed through NASA Global Change Master Directoryhttp://gcmd.gsfc.nasa.gov/index.html (last visited on July 31st 2015).

Table 3
H_s errors corresponding to the different parameterizations of $S_{in} + S_{ds}$. The references are altimetric data in the Atlantic region. The simulated period was 1/1/2005–30/6/2005. 2223 data points were obtained for comparison. Bias and RMSE are in m, and SI is dimensionless.

	Bias (m)	RMSE (m)	SI
WAM-3	−0.20	0.37	18.4
Tolman and Chalikov	−0.16	0.34	17.6
WAM-4 and variants	−0.15	0.34	17.5

3. Results and discussion

3.1. Model calibration and validation

Table 3 shows the results obtained with different parameterizations of $S_{in} + S_{ds}$. The package WAM-4 performs better for the three error metrics used. The results obtained with this parameterization are shown in Fig. 4a.

Calibration of the WAM-4 package results in $C_{ds} = -1.5$. Fig. 4b and Table 4 show that with this value, the of H_s is nearly zero. Table 4 and Fig. 4c also show the validations results. The model performance in validation and calibration was similar; therefore, the obtained results are considered satisfactory.

Table 5 shows the H_s errors obtained in the Río de la Plata (RDP). Although the estuary was not considered in the $S_{in} + S_{ds}$ selection and model calibration, the results obtained in the outer RDP (altimeter and buoy) are as good as those obtained in the Atlantic region (Table 5). Fig. 5 shows the agreement of the comparisons between the model results and in situ measurement time series.

3.2. Wave power spatial distribution and wave climate characteristics

The mean wave power map is shown in Fig. 6, and the maps of the 25th, 50th, 75th and 99th wave power percentiles are shown in Fig. 7.

These maps show a similar pattern: a SE–NW gradient and a strong decay inside the estuary. The Atlantic region has values of 30 kW/m at 200 km offshore and 20 kW/m at 70 km offshore, and at 20 m depth (where virtual buoys B1 – B17 are located) the mean wave power varies between 8 and 14 kW/m. In the RDP, the mean wave power decreases from 7 kW/m in the outer zone to 1 kW/m in the mid zone and continues decreasing towards the inner zone. On the Atlantic coast, wave power northward of La Paloma is higher than between Punta del Este and La Paloma. This is shown in Fig. 8 and Table 6.

Table 4
H_s errors obtained with the calibrated model and its validation in the Atlantic region.

	Bias (m)	RMSE (m)	SI
Calibration	0.02	0.29	17.3
Validation	0.06	0.30	16.9

Table 5
H_s errors in the Río de la Plata.

	Bias (m)	RMSE (m)	SI
Outer RDP	−0.05	0.28	27.8
Inner and middle RDP	−0.25	0.35	33.8
Buoy	0.09	0.28	22.5
ADCP	0.04	0.26	50.2

On the Atlantic coast, the mean wave power varies between 10 and 14 kW/m in the Chuy to La Paloma stretch (B1 to B12), whereas in the La Paloma to Punta del Este stretch (B13 to B17), the mean wave power varies between 8 and 10 kW/m (see Fig. 8 and Table 6. Integrating these results along the 200 km covered between B1 and B17, a total of 2.2 GW is obtained. This figure is the theoretical wave energy potential of the Atlantic coast at 20 m depth. While technology constraints and coastal use conflicts imply that only a fraction of this potential could be exploited, the value is double the current electric energy consumption of the country.

Based on these results, the study area is classified into three zones, and a virtual buoy representative of each one is selected: Atlantic coast between Chuy and La Paloma (virtual buoy B6), Atlantic coast between La Paloma and Punta del Este (virtual buoy B15) and outer Rio de la Plata (virtual buoy B19). Wave power roses and annual wave energy distribution in terms of significant wave height and period Tm01 corresponding to these three points are presented in Figs. 9 and 10, respectively.

Fig. 10 shows that in the three analyzed buoys, predominant waves (those with the highest annual frequency) are the largest contributors to wave energy potential, i.e., the most frequent waves are the major contributors to the mean annual energy. This is a positive factor in terms of resource availability because it implies that the wave energy is well distributed in time. These frequent waves on the Atlantic coast have significant wave heights in the range of 0.8 and 1.8 m and periods T_{m01} in the range of 6 and 9 s. These waves are spread in the E–S quadrant (see Fig. 9).

Lastly, Fig. 11 shows the average wave energy spectrums for the three analyzed points. The average spectrum of B6 has the energy distributed in the E–S quadrant and concentrated in periods between 9 and 13 s. The average spectrum of B15 is similar to B6, but

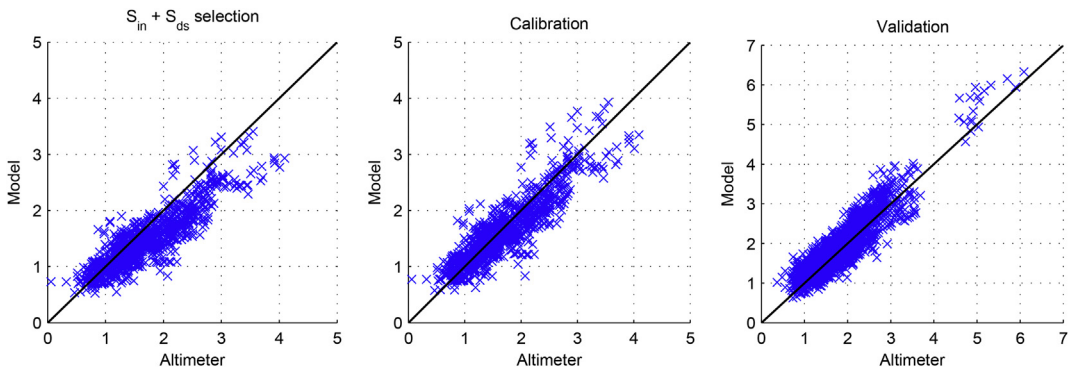

Fig. 4. Significant wave height in meters (H_s(m)). Model result vs altimeter data in the Atlantic region. a) WAM-4 and variants, $C_{ds} = -2.1$, 1/1/2005–30/6/2005; b) WAM-4 and variants, $C_{ds} = -1.5$, 1/1/2005–30/6/2005; c) WAM-4 and variants, $C_{ds} = -2.1$, 1/7/2005–31/12/2005.

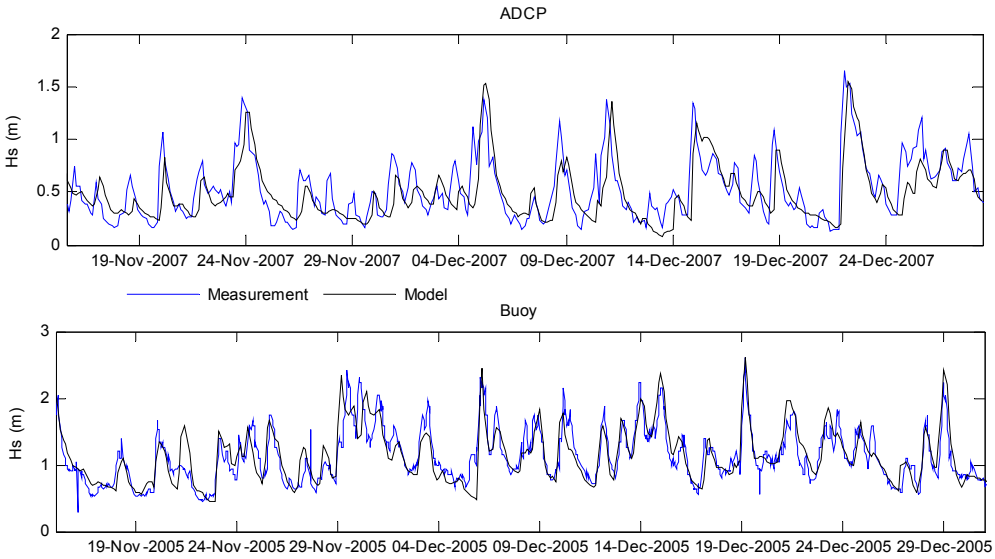

Fig. 5. Comparison of the model H_s results and the measured time series.

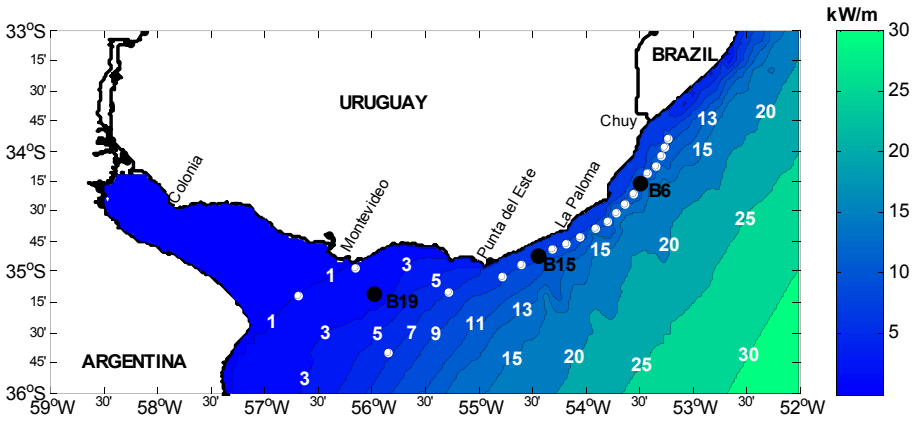

Fig. 6. Spatial distribution of the mean wave power.

the energy is more widely spread in periods and shifted to the west, with a considerable portion of energy in the S–W quadrant. The average spectrum of B19 has a different pattern, with energy more widely spread both in direction and period.

3.3. Temporal variability

Fig. 12 shows the COV (coefficient of variability) maps obtained for the different time scales considered: sea state (3h), monthly and annual.

For the sea states, the coefficient (COV_3h) is approximately 1.2. Compared with [9]; these results are significantly lower than the results obtained for the northern hemisphere, where COV_3h > 1.5, but are higher than the prevailing results obtained for the southern hemisphere, where COV_3h < 0.8. Between La Paloma and Chuy, COV_3h is lower than between Punta del Este and La Paloma and inside the estuary. This pattern is also observed for COV_monthly and COV_annually, that is, La Paloma-Chuy has the lowest wave power variability of the three zones for all analyzed time scales.

Particularly noteworthy is the low annual variability. At no point is COV_annually higher than 0.1, indicating that the standard deviation of the annual mean energy is less than the 10% of the mean annual energy for the whole area. This is also shown in Fig. 13, where the annual mean wave power throughout the simulated period is presented for the three buoys considered.

The maps of the MV (monthly variability) index and SV (seasonality variability) index are shown in Fig. 14. On the Atlantic coast, MV and SV are in the range of 0.5–0.6 and 0.3–0.45, respectively. These results reflect the low wave power variability of the study zone at this timescale. Compared with [9]; this area is among the sites with the lowest wave power monthly and seasonal variability; typically MV > 1.5 and SV > 1.25 for the northern hemisphere, whereas in the southern hemisphere, MV is mostly between 0.6 and 0.9 and SV is between 0.5 and 1.

Fig. 15 presents the mean wave power annual cycle for the three considered buoys. The low monthly variability is noted, and September and January are the most (P_{M1}) and the least (P_{M12}) energetic months, respectively. Fig. 16 presents the seasonal wave power roses for each considered buoy. In autumn (AMJ) and winter (JAS), the wave energy is higher than in spring (OND) and summer (JFM), but the difference is moderate. The wave energy during cold seasons (AMJ + JAS) is approximately 55%–60% of the total annual energy. However, a significant seasonal variability is observed for wave directions, with eastern waves being more frequent during hot seasons (OND + JFM). This directional

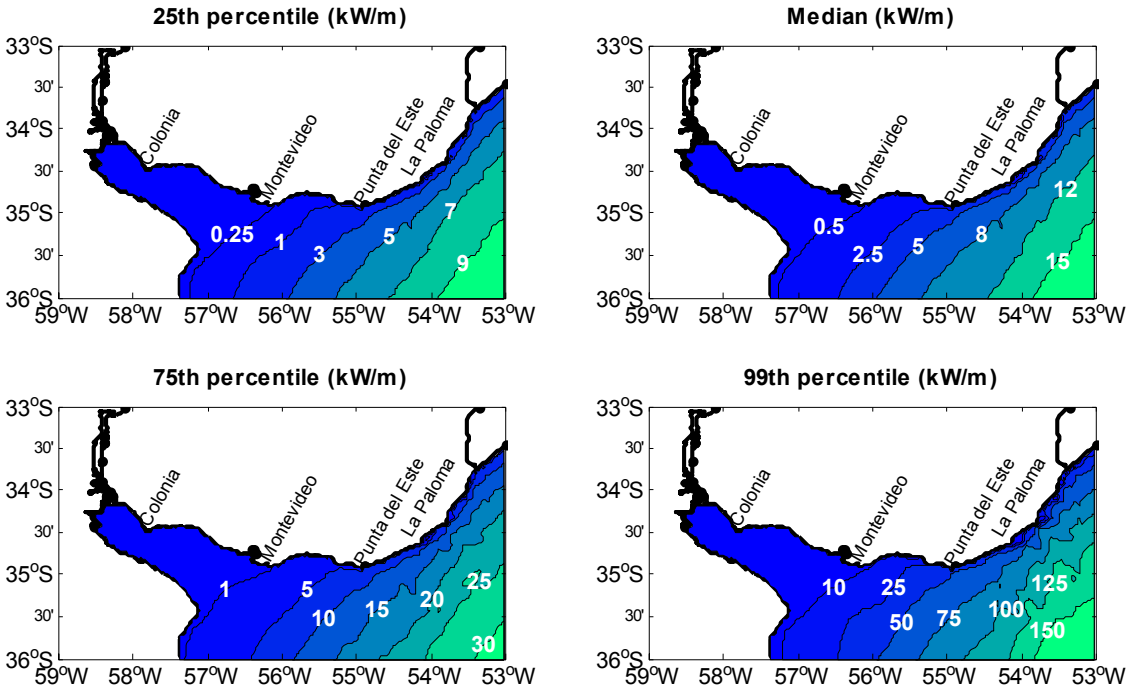

Fig. 7. Wave power 25th, 50th, 75th and 99th percentiles.

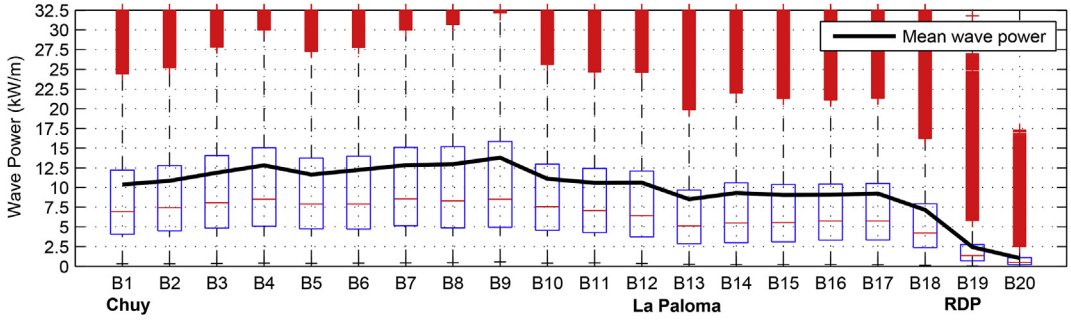

Fig. 8. Box plot of the wave power at each virtual buoy.

Table 6
Depth, mean significant wave height, 99% quantile significant wave height and mean wave power at each virtual buoy. The points considered hereinafter for the detailed analysis are labeled in bold.

Point	Depth (m)	$(H_s)_{mean}$ (m)	H_{99} (m)	P_{mean} (kW/m)
B1	16.2	1.4	3.0	10.4
B2	18.4	1.5	3.0	10.9
B3	17.5	1.5	3.3	11.9
B4	17.9	1.6	3.3	12.8
B5	20.1	1.5	3.2	11.7
B6	**15.1**	**1.5**	**3.2**	**12.2**
B7	12.4	1.5	3.4	12.8
B8	14.8	1.5	3.5	13.0
B9	16.5	1.6	3.7	13.8
B10	30.8	1.5	3.2	11.1
B11	21.7	1.4	3.2	10.6
B12	12.0	1.4	3.3	10.6
B13	23.5	1.3	3.1	8.5
B14	25.3	1.3	3.1	9.3
B15	**26.2**	**1.3**	**3.1**	**9.1**
B16	29.4	1.3	3.2	9.1
B17	27.0	1.3	3.2	9.3
B18	22.2	1.2	3.1	7.2
B19	**9.1**	**0.8**	**2.1**	**2.4**
B20	6.6	0.6	1.8	1.0

variability is not quantified in the MV and SV indexes that focus only on the magnitude of the wave power, not on its direction (see Fig. 16).

Finally, the correlation between the monthly wave energy anomaly and several climatic indexes was analyzed. Table 7 shows the obtained results. Antarctic Oscillation is the only index that has a statistically significant correlation with the monthly wave energy anomaly at the three analyzed buoys. For the northern stretch of the Atlantic Ocean, significant correlation with the Southern Oscillation Index is also obtained. This is in agreement with previous results [50]. Only the AAO and SOI indexes are used for the analysis of the monthly wave energy

Table 7
Linear correlation between the monthly wave energy anomaly and climatic indexes. Only correlations statistically significant at the 90% level are shown (correlations significant at the 95% level are labeled in bold).

Buoy	Climatic index			
	AAO	TSA	Nino 3.4	SOI
B6	0.10	–	–	−0.10
B15	**0.12**	–	–	–
B19	**0.11**	–	–	–

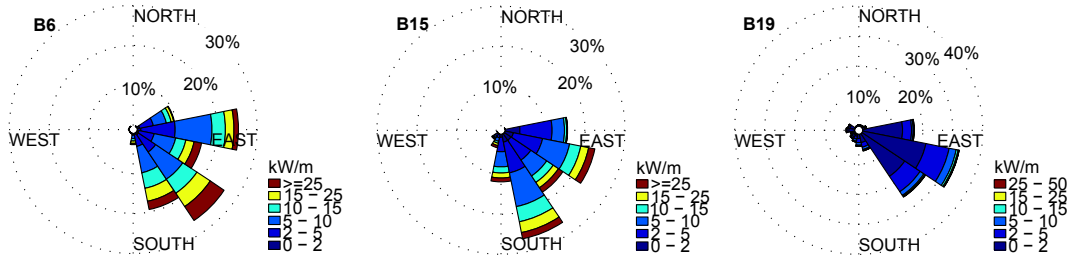

Fig. 9. Wave power roses at B6, B15 and B19.

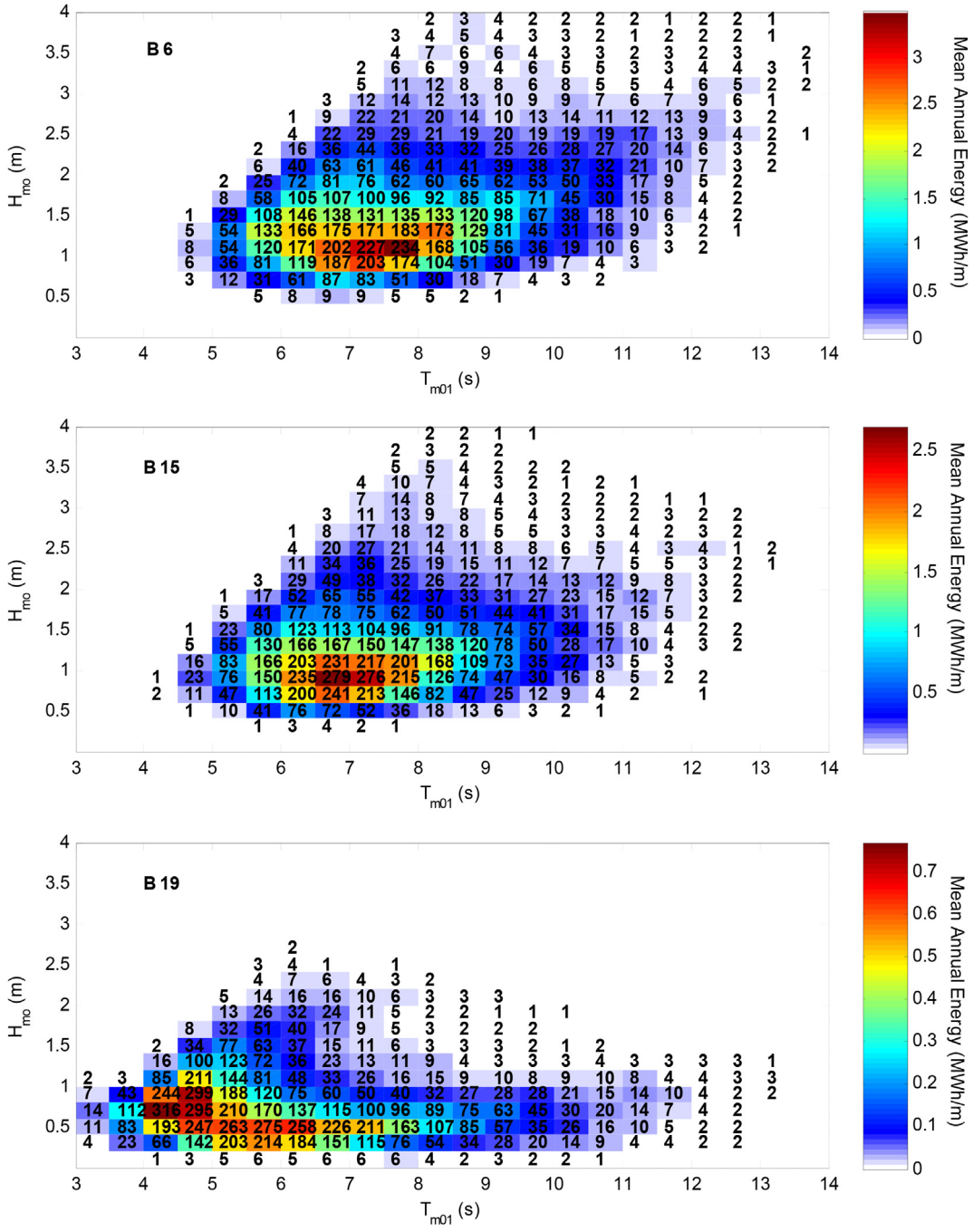

Fig. 10. Annual wave energy distribution in terms of significant wave height Hm0 and period Tm01 at B6, B15 and B19. The color scale represents annual wave energy, and the numbers represent the occurrence of the different sea states in hours per year. (For interpretation of the references to colour in this figure legend, the reader is referred to the web version of this article.)

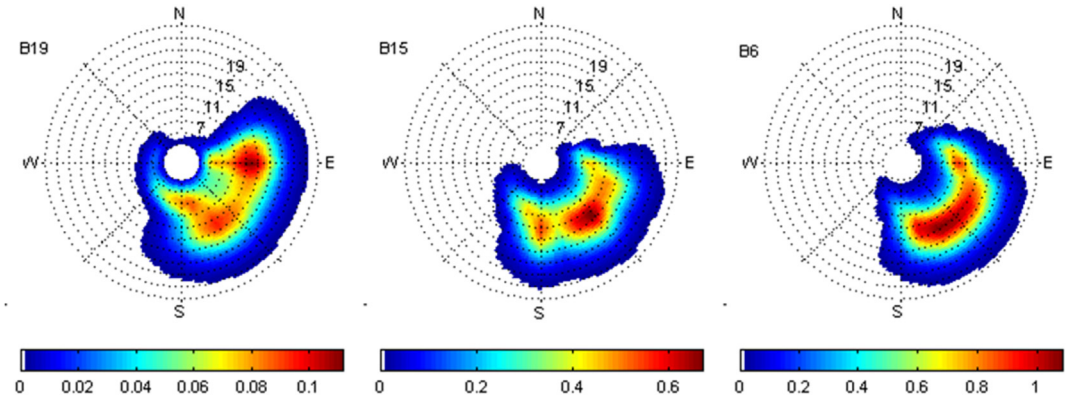

Fig. 11. Average wave energy spectrum at B6 (La Paloma – Chuy), B15 (Punta del Este – La Paloma) and B19 (outer Rio de la Plata) in $m^2/(Hz^*rad)$.

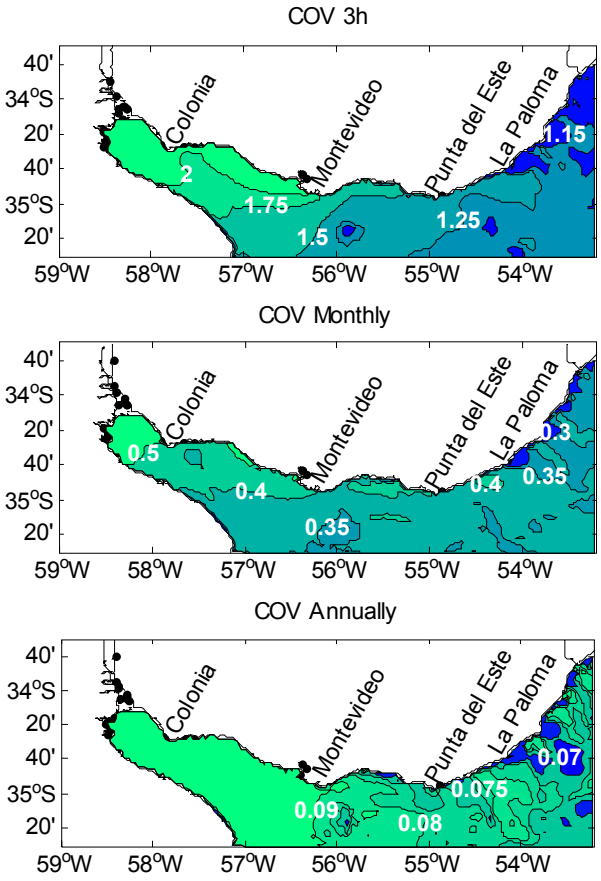

Fig. 12. Maps of the variability coefficients at different time scales.

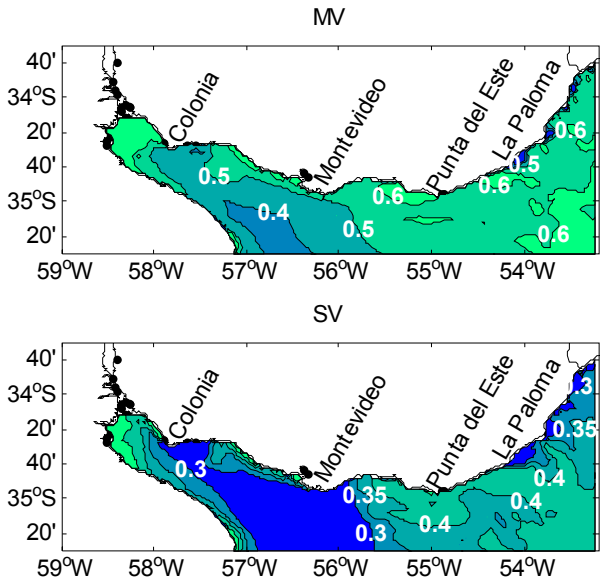

Fig. 14. Maps of monthly variability index (MV) and sesonality variability index (SV).

variability at each spectral bin. Fig. 17 shows the obtained results. For the three buoys, a positive AAO anomaly is associated with an increase in the energy content for the low period eastern bins and a decrease in the high period southern bins, whereas a positive SOI anomaly is associated with a decrease in the high period south-southeastern bins. Moreover, both AAO and SOI affect the modes of the spectrums, except for B6, for which only SOI affects its main mode.

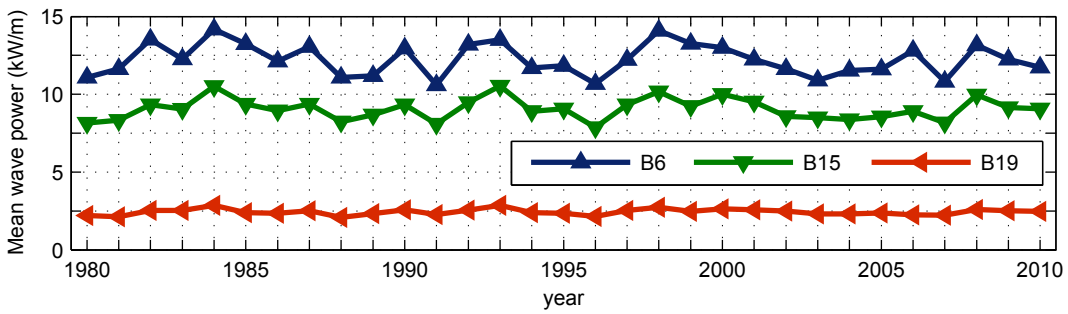

Fig. 13. Annual mean wave power at B6, B15 and B19.

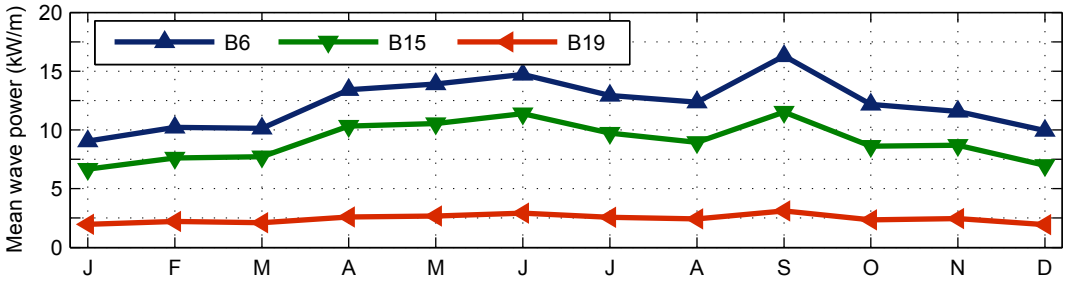

Fig. 15. Monthly mean wave power at B4, B9, B15 and B19.

3.4. Extreme wave climate

The map of the ETER index is presented in Fig. 18. Higher values of the index are obtained for the La Paloma-Chuy stretch than for the La Paloma-Punta del Este stretch. This is an advantage of the former zone over the latter (the closer the index is to 100, the closer are the exploitation and the design waves).

Fig. 19 shows the map of H_{10}. A comparison with similar results obtained by previous authors for other sites (e.g., global map in Ref. [9] shows that the severity of extreme waves is lower here than in the most template coasts in the world, particularly those in the northern hemisphere.

4. Conclusions

A detailed assessment of wave energy resources in Uruguay was presented. The analysis was performed on the basis of a 31-year wave hindcast conducted with the WAVEWATCH III® wave model forced with CFSR winds. The assessment includes the wave power spatial distribution, a temporal variability analysis of different timescales, the relation with climate indexes and considerations of extreme events.

The obtained results show that the mean wave power in deep water is 30 kW/m. Although the potential diminishes towards the coast, on the Atlantic coast, at a 20 m depth, the theoretical potential doubles the current electrical energy consumption of the country. Meanwhile, the wave power in the Río de la Plata decays from 7 kW/m in the outer zone to 1 kW/m in the intermediate zone and continues decreasing toward the inner zone.

The prevailing sea states are those that contribute the most to the mean annual wave energy. Regarding temporal variability, the results show low medium- and long-term (monthly, seasonal and annual) variability but not as low variability in the short-term (sea state time scale). Moreover, seasonal variability related to wave direction was detected. With respect to extreme events, the 10-year

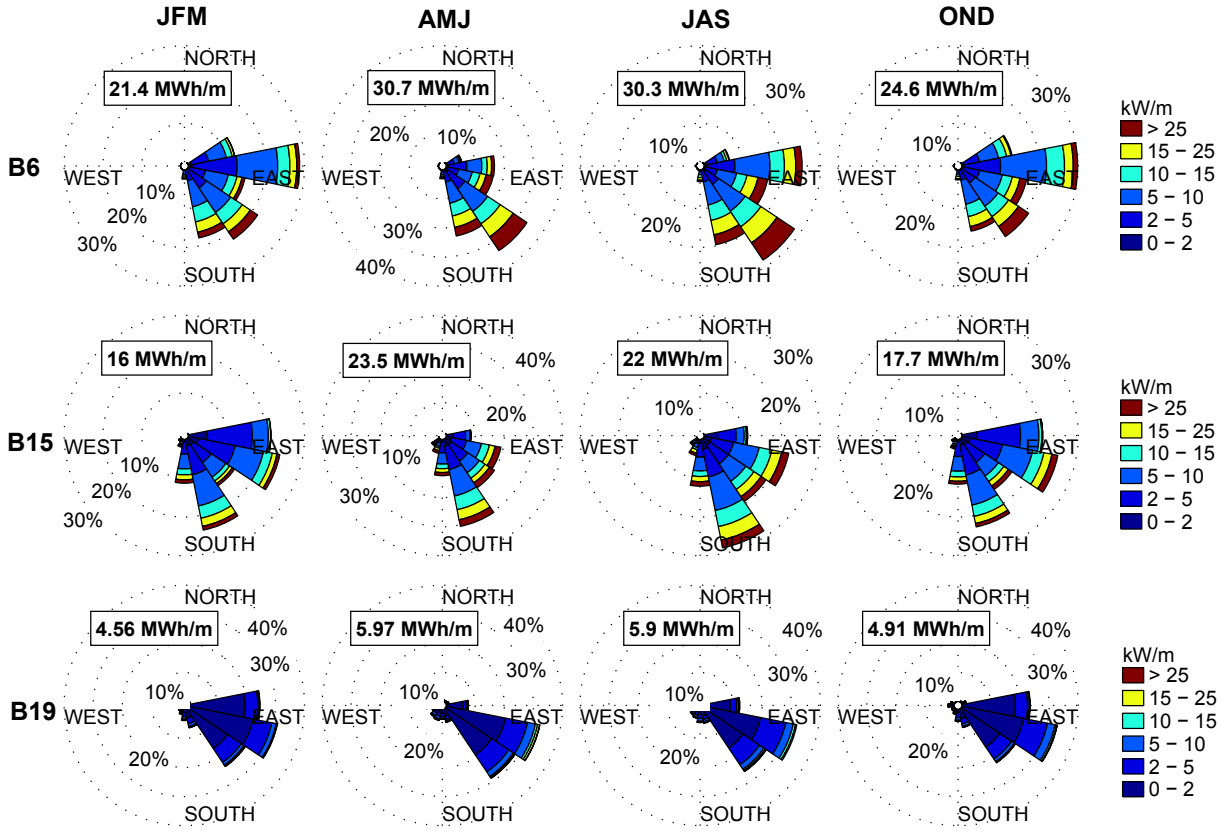

Fig. 16. Seasonal wave power roses at B6, B15 and B19.

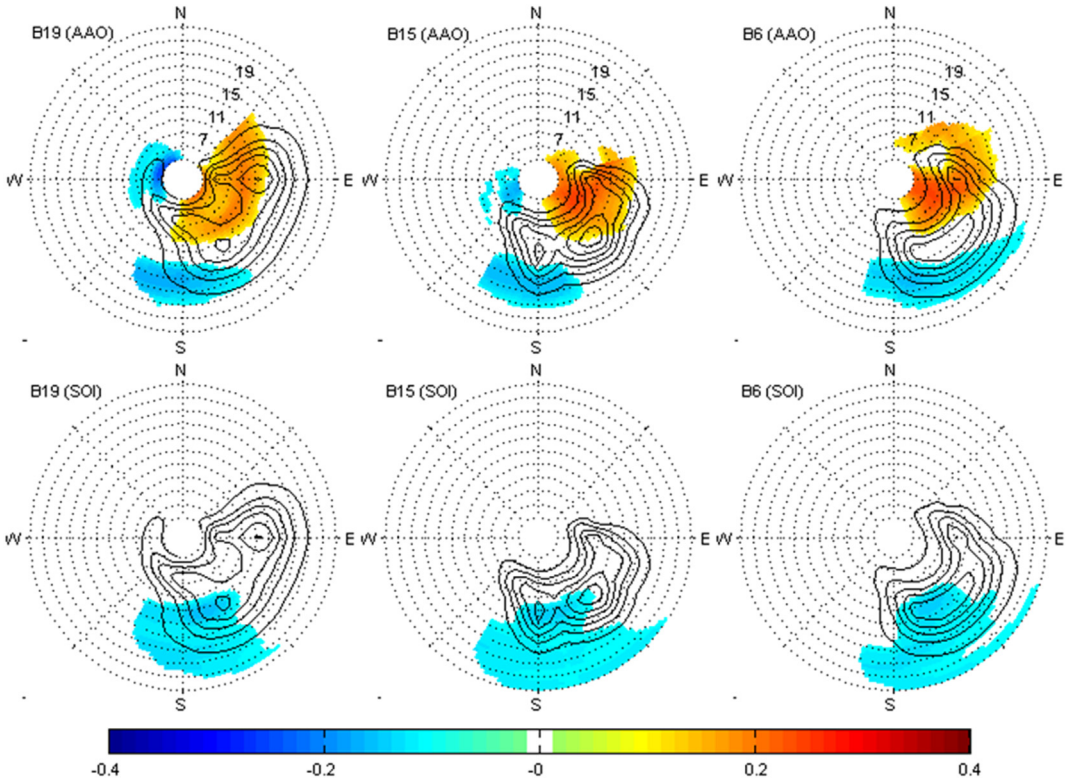

Fig. 17. Linear correlation between the monthly wave energy anomaly at each spectral bin and the AAO and SOI indexes. Black contour lines correspond to the mean annual energy spectrum at each buoy. Only the correlations statistically significant at the 95% level are shown.

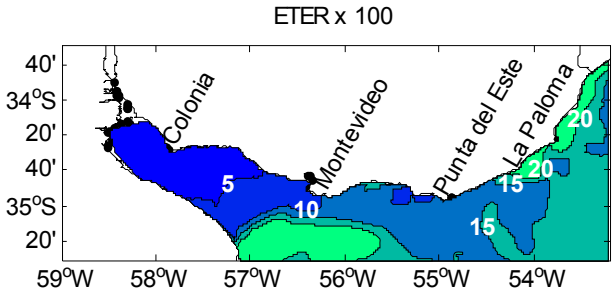

Fig. 18. Exploitation to extreme ratio (ETER) index map.

return period significant wave height is not too severe when compared with other areas analyzed by previous authors.

Although the aforementioned aspects of wave energy resource apply to the whole Atlantic coast, La Paloma–Chuy is the stretch of coast with the highest wave energy potential, the least variability and the highest values of the ETER index. The variability within the directional wave energy spectrum has less influence on the mode of the spectrum on this stretch of coast than on the others. For these reasons, La Paloma-Chuy is considered to be the most attractive stretch of Uruguayan coast for wave energy development.

In summary, this assessment has shown that although the wave energy potential in Uruguay is moderate, it is fairly steady throughout the year, and the extreme wave conditions are relatively benign.

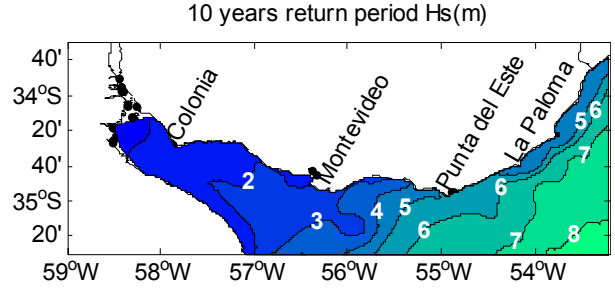

Fig. 19. Ten-year return period significant wave height (H_{10}).

Acknowledgments

This work was partially founded by the Uruguayan Agency for Research and Innovation (ANII) through its Energy Funds program (FSE), contract numbers PR-FSE-2009-1-12 and FSE-1-2013-1-10748. Rodrigo Alonso acknowledges the financial support provided by ANII through the postgraduate scholarships program, grant number POS-NAC-2012-1-8936. Sebastián Solari acknowledges the financial support provided by ANII through the postdoctoral scholarship "Fondo Profesor Dr. Roberto Caldeyro Barcia", grant number PD-NAC-2012-1-7829.

Appendix 1. Extreme wave analysis

Extreme wave analysis is performed following the annual maxima approach. To this end, an annual maxima data series is obtained at each grid point and is used for fitting a GEV (Generalized Extreme Value) distribution (see e.g., [8]).

$$G(z) = exp\left\{ -\left[1 + \xi\left(\frac{z-\mu}{\sigma}\right)\right]^{-1/\xi}\right\}$$

where $-\infty < \mu < \infty$ is the location parameter, $\sigma > 0$ is the scale parameter, $-\infty < \xi < \infty$ is the shape parameter and the function is defined on the set $\{z:1 + \xi(z - \mu)/\sigma > 0\}$.

The parameters of the GEV distribution are estimated for every grid point using PWM (Probability Weighted Moments), following [25] $\xi = -(7.859c + 2.955c^2)$.

$$\sigma = -\frac{(2b_1 - b_0)\xi}{\Gamma(1-\xi)(1-2^{\xi})}$$

$$\mu = b_0 - \sigma\{\Gamma(1-\xi) - 1\}/\xi$$

with b_0, b_1 and c estimated from the annual maxima data series as,

$$b_i = n^{-1}\sum_{j=1}^{n} p_{j,n}^{r} x_j$$

$$c = \frac{2b_1 - b_0}{3b_2 - b_0} - \frac{\log 2}{\log 3}$$

where x_j is the ordered sample of n elements ($x_1 \leq \ldots \leq x_j \leq \ldots \leq x_n$), and $p_{j,n}$ is the plotting position, estimated as,

$$p_{j,n} = \frac{j - 0.35}{n}$$

References

[1] Akpınar A, Kömürcü Mİ. Assessment of wave energy resource of the Black Sea based on 15-year numerical hindcast data. Appl Energy 2013;101:502–12.
[2] Ayat B. Wave power atlas of eastern Mediterranean and Aegean seas. Energy 2013;54:251–62.
[3] Appendini CM, Urbano-Latorre CP, Figueroa B, Dagua-Paz CJ, Torres-Freyermuth A, Salles P. Wave energy potential assessment in the Caribbean low level jet using wave hindcast information. Appl Energy 2015;137:375–84.
[4] Bento AR, Martinho P, Soares CG. Numerical modelling of the wave energy in Galway Bay. Renew Energy 2015;78:457–66.
[5] Carballo R, Sánchez M, Ramos V, Fraguela JA, Iglesias G. Intra-annual wave resource characterization for energy exploitation: a new decision-aid tool. Energy Convers Manag 2015a;93:1–8.
[6] Carballo R, Sánchez M, Ramos V, Fraguela JA, Iglesias G. The intra-annual variability in the performance of wave energy converters: a comparative study in N Galicia (Spain). Energy 2015b;82:138–46.
[7] Chawla A, Spindler DM, Tolman HL. Validation of a thirty year wave hindcast using the climate forecast system reanalysis winds. Ocean Model 2013;70:189–206.
[8] Coles S. An introduction to statistical modeling of extreme values (Springer series in statistics). Springer-Verlang London Limited; 2001. ISBN: 1-85233-459-2.
[9] Cornett AM. A global wave energy resource assessment. In: Proceedings of the Eighteenth (2008) International Offshore and Polar Engineering Conference; 2008.
[10] Davis RW, Moore EF. A numerical study of vortex shedding from rectangles. J Fluid Mech 1982;116:475–506.
[11] Defne Z, Haas KA, Fritz HM. Wave power potential along Atlantic coast Southeast USA. Renew Energy 2009;34:2197–205.
[12] Esteban M, Leary D. Current developments and future prospects of offshore wind and ocean energy. Appl Energy 2012;90:128–36.
[13] Falcão AF de O. Wave energy utilization: a review of the technologies. Renew Sustain Energy Rev 2010;14:899–918.
[14] García-Medina G, Özkan-Haller HT, Ruggiero P. Wave resource assessment in Oregon and southwest Washington, USA. Renew Energy 2014;64:203–14.
[15] Gonçalves M, Martinho P, Guedes Soares C. Wave energy conditions in the western French coast. Renew Energy 2014a;62:155–63.
[16] Gonçalves M, Martinho P, Guedes Soares C. Assessment of wave energy in the Canary Islands. Renew Energy 2014b;68:774–84.
[17] Gunn K, Stock-Williams C. Quantifying the global wave power resource. Renew Energy 2012;44:296–304.
[18] Gutiérrez A, Cataldo J, Cazes Boezio G. WRF-ARW application to forecasting wind energy, with sensibility of topography. In: International Conference on Wind Engineering. (13rd. : 2011, Amsterdam); 2011.
[19] Hagerman G. Oceanographic design criteria and site selection for ocean wave energy conversion. In: Evans DV, Falcao AFde O, editors. Hydrodynamics of ocean wave-energy utilization. Springer-Verlag; 1985. ISBN-13:978-3-642-82668-9.
[21] Hasselmann S, Hasselmann K. Computations and parameterizations of the nonlinear energy transfer in a gravity-wave spectrum. Part I: a new method for efficient computations of the exact nonlinear transfer integral. J Phys Oceanogr 1985;15:1369–77.
[22] Hasselmann K, Barnett TP, Bouws E, Carlson H, Cartwright DE, Enke K, et al. Measurements of wind-wave growth and swell decay during the JointNorthSeaWave Project (JONSWAP). Ergaenzungsheftzur Deutschen Hydrographischen Zeitschrift, Reihe A 1973;12(8). 95pp.
[23] Hayward J, Behrens S, Mcgarry S, Osman P. Economic modelling of the potential of wave energy. Renew Energy 2012;48:238–50.
[24] Holthuijsen LH. Waves in oceanic and coastal waters. Cambridge University Press; 2007. ISBN 9781139462525.
[25] Hosking JRM, Wallis JR, Wood EF. Estimation of the generalized extreme-value distribution by the method of probability-weighted moments. Technometrics 1985;27:251–61.
[26] Hughes MG, Heap AD. National-scale wave energy resource assessment for Australia. Renew Energy 2010;35:1783–91.
[27] ISO 19901-1. Petroleum and natural gas industries — specific requirements for offshore structures — Part 1: metocean design and operating considerations. 2005.
[28] Kim G, Jeong WM, Lee KS, Jun K, Lee ME. Offshore and nearshore wave energy assessment around the Korean Peninsula. Energy 2011;36:1460–9.
[29] Komen GJ, Cavaleri L, Donelan M, Hasselmann K, Hasselmann S, Janssen PAEM. Dynamic and modelling of ocean waves. Cambridge University Press; 1996. ISBN 9780521577816.
[30] Lenee-Bluhm P, Paasch R, Özkan-Haller HT. Characterizing the wave energy resource of the US Pacific Northwest. Renew Energy 2011;36:2106–19.
[31] Leonard BP. A stable and accurate convective modelling procedure based on quadratic upstream interpolation. Comput Methods Appl Mech Eng 1979;19:59–98.
[32] Leonard BP. The ULTIMATE conservative difference scheme applied to unsteady one-dimensional advection. Comput Methods Appl Mech Eng 1991;88:17–74.
[33] Liberti L, Carillo A, Sannino G. Wave energy resource assessment in the Mediterranean, the Italian perspective. Renew Energy 2013;50:938–49.
[34] Mackay EBL, Bahaj AS, Challenor PG. Uncertainty in wave energy resource assessment. Part 1: historic data. Renew Energy 2010a;35(8):1792–808.
[35] Mackay EBL, Bahaj AS, Challenor PG. Uncertainty in wave energy resource assessment. Part 2: variability and predictability. Renew Energy 2010b;35(8):1809–19.
[36] Ministerio de Industria Energía y Minería -Dirección Nacional de Energía (MIEM-DNE). Políticas Energéticas 2005–2030. 2012. Report (In Spanish), http://www.dne.gub.uy/documents/49872/0/Pol%C3%ADtica%20energ%C3%A9tica%202005-2030?version=1.0&t=1378917147456.
[37] Mirzaei A, Tangang F, Juneng L. Wave energy potential along the east coast of Peninsular Malaysia. Energy 2014;68:722–34.
[38] Monteforte M, Lo Re C, Ferreri GB. Wave energy assessment in Sicily (Italy). Renew Energy 2015;78.
[39] Mørk G, Barstow S, Kabuth A, Pontes MT. Assessing the global wave energy potential. In: Proceedings of OMAE2010 29th International Conference on Ocean, Offshore Mechanics and Arctic Engineering; 2010.
[40] Neill SP, Hashemi MR. Wave power variability over the northwest European shelf seas. Appl Energy 2013;106:31–46.
[41] Neill SP, Lewis MJ, Hashemi MR, Slater E, Lawrence J, Spall SA. Inter-annual and inter-seasonal variability of the Orkney wave power resource. Appl Energy 2014;132:339–48.
[42] Ortega S, Osorio AF, Agudelo P. Estimation of the wave power resource in the Caribbean Sea in areas with scarce instrumentation. Case study: Isla Fuerte, Colombia. Renew Energy 2013;5:240–8.
[43] Rusu L, Guedes Soares C. Wave energy assessments in the Azores islands. Renew Energy 2012;45:183–96.
[44] Saket A, Etemad-Shahidi A. Wave energy potential along the northern coasts of the Gulf of Oman, Iran. Renew Energy 2012;40:90–7.
[45] Sierra JP, Mösso C, González-Marco D. Wave energy resource assessment in Menorca (Spain). Renew Energy 2014;71:51–60.
[46] Soomere T, Eelsalu M. On the wave energy potential along the eastern Baltic Sea coast. Renew Energy 2014;71:221–33.
[47] Stopa JE, Cheung KF, Chen Y-L. Assessment of wave energy resources in Hawaii. Renew Energy 2011;36:554–67.
[48] Saha S, Moorthi S, Pan H-L, Wu X, Wang J, Nadiga S, et al. The NCEP Climate Forecast System Reanalysis. Bull Am Meteorol Soc 2010;91:1015–57.
[49] Soerensen HS, Weinstein A. "Ocean energy position paper for IPCC" (paper presented at the proceeding of IPCC scoping meeting on renewable energy sources, Lubeck, Germany, P5). 2008.
[50] Solari S, Losada MA. Parametric and non-parametric methods for the study of the variability of wave directions: application to the Atlantic Uruguayan coasts. In: Proceedings of 33th International Conference on Coastal Engineering, ASCE; 2012.
[51] Suarez RA, Toscano P, Siri R, Musé P, Abal G. Recent advances in solar resource assessment in Uruguay. Transm Distrib Lat Am Conf Expo (T&D-LA) 2012. 2012 Sixth IEEE/PES.
[52] The Carbon Trust. Future marine energy. Results of the marine energy challenge: cost competitiveness and growth of wave and tidal stream energy. 2006. Report.

[53] Tiwari NW, Mishra RK. Advances renewable energy source. RSC Publishing; 2011. p. 586.
[54] Tolman HL. Alleviating the garden sprinkler effect in wind wave models. Ocean Model 2002;4:269–89.
[55] Tolman HL. User manual and system documentation of wavewatch III version 3.14.Tech. Note 276, NOAA/NWS/NCEP/MMAB. 2009. p. 220.
[56] Van Nieuwkoop JCC, Smith HCM, Smith GH, Johanning L. Wave resource assessment along the Cornish coast (UK) from a 23-year hindcast dataset validated against buoy measurements. Renew Energy 2013;58:1–14.
[57] Waters R, Engström J, Isberg J, Leijon M. Wave climate off the Swedish west coast. Renew Energy 2009;34:1600–6.
[58] Wu S, Liu C, Chen X. Offshore wave energy resource assessment in the East China Sea. Renew Energy 2015;76:628–36.
[59] Bahaj AS. Generating electricity from the oceans. Renewable and Sustainable Energy Reviews 2011;15(7):3399–416. http://doi.org/10.1016/j.rser.2011.04.032.
[60] Battjes Jaa, Janssen JPFMPFM. Energy loss and set-up due to breaking of random waves. Proceedings of the 16th International Conference on Coastal Engineering 1978;1(16):569–87. http://doi.org/10.9753/icce.v16.
[61] Iglesias G, Carballo R. Wave energy potential along the Death Coast (Spain). Energy 2009;34(11):1963–75. http://doi.org/10.1016/j.energy.2009.08.004.
[62] Iglesias G, Carballo R. Wave power for La Isla Bonita. Energy 2010;35(12):5013–21. http://doi.org/10.1016/j.energy.2010.08.020.
[63] Iglesias G, Carballo R. Wave resource in El Hierro-an island towards energy self-sufficiency. Renewable Energy 2011;36(2):689–98. http://doi.org/10.1016/j.renene.2010.08.021.
[64] WISE group. Wave modelling — The state of the art. Progress in Oceanography 2007;75(4):603–74. http://doi.org/10.1016/j.pocean.2007.05.005.